Biochimica et Biophysica Acta, 1070 (1991) 33–42

BBAMEM 75432

The effect of monoacylglycerol on the phase behavior of egg phosphatidylcholine

C.-C. Yin [1], P. Schurtenberger [2], E. Wehrli [3], F. Paltauf [4] and H. Hauser [1]

[1] *Laboratorium für Biochemie,* [2] *Institut für Polymere und* [3] *Laboratorium für Elektronenmikroskopie I, Institut für Zellbiologie, Eidgenössische Technische Hochschule Zürich, ETH-Zentrum, Zürich (Switzerland) and* [4] *Institut für Biochemie und Lebensmittelchemie, Technische Universität Graz, Graz (Austria)*

(Received 15 May 1991)

Key words: Monoacylglycerol; Phosphatidylcholine; Phase behavior; NMR, ^{31}P-; Freeze-fracture; Dynamic light scattering

Phosphatidylcholine bilayers can accommodate large quantities of monoacylglycerol. Incorporating up to 40% monoacylglycerol has little effect on the orientation and motion of the phosphatidylcholine polar group. Briefly heating mixed dispersions of 1-monooleoylglycerol / egg phosphatidylcholine (1 : 1, weight ratio; 2.1 : 1, mole ratio) to 50–60 °C induced spontaneous vesiculation: unilamellar and some oligolamellar vesicles bud off the large multilamellar particles. The size of the resulting vesicles ranges from 100 to 1000 nm, with the bulk of the vesicles having diameters between 100 and 500 nm. The spontaneous vesiculation process is reflected in the visual clearance of the mixed lipid dispersion and in the collapse of the ^{31}P powder NMR spectrum to a sharp, asymmetric peak. The narrowing of the ^{31}P-NMR spectrum is explained in terms of additional molecular and / or segmental motion of the lipid polar groups. In mixed dispersions of 1-monooleoylglycerol / egg phosphatidylcholine containing an excess of 1-monooleoylglycerol (≥ 50%) domain formation takes place, i.e., the formation of local clusters enriched in either of the two lipids. As a result the mechanical properties of these mixed lipid bilayers seem to be quite different from those of pure egg phosphatidylcholine.

Introduction

Monoacylglycerols are amphiphiles that are of both industrial and biological importance. In the food industry racemic mixtures of 1-monoacyl- and 2-monoacylglycerols have been widely used as emulsifiers. These compounds also serve as the starting material for the synthesis of more complex emulsifiers and detergents.

It is now well established that the main products of fat or triacylglycerol digestion in the small intestine are partially ionized fatty acids and 2-monoacyl-*sn*-glycerols [1]. The hydrolysis of triacylglycerols is enzymatically catalyzed by gastric and pancreatic lipases [2–4]. Since the aqueous solubility of partially ionized long-chain fatty acids and monoacylglycerols is low, i.e., in the nanomolar to micromolar range, the lipolytic products have to be emulsified and transported to the site of lipid absorption. This site is the brush border membrane of the epithelial cells (enterocytes). Bile salts are the prime emulsifyer and the resulting mixed bile salt micelles are considered to be the main transport vehicle of the lipolytic products [5]. Considering that 100 to 150 g triacylglycerols are consumed daily by an average western adult [1], rather large quantities of 2-monoacyl-*sn*-glycerols may be present, though transiently, in the intestinal lumen, in the brush border membrane during fat absorption and in the cytoplasm of the enterocyte after the absorptive process. Monoacylglycerols are also important intermediates of the cell's triacylglycerol catabolism and anabolism.

Here we study the effect of increasing quantities of monoacylglycerol on the smectic (lamellar) phase of aqueous egg phosphatidylcholine dispersions. Egg phosphatidylcholine bilayers present in excess water serve as model membranes to explore the effect of increasing amounts of monooleoylglycerol. We address

Abbreviations: EPC, egg phosphatidylcholine; ^{3}H-DPPC, 1,2-dipalmitoyl-*sn*-phosphatidyl[*N-methyl*-^{3}H(U)]choline; MOG, 1-monooleoyl-*sn*-glycerol or 1-monooleoyl-*rac*-glycerol; EDTA, ethylenediaminetetraacetic acid; Tris, tris(hydroxymethyl)aminoethane; QLS, quasielastic light scattering.

Correspondence: H. Hauser, Laboratorium für Biochemie, ETH-Zentrum, Universitätstrasse 16, CH-8092 Zürich, Switzerland.

the question of membrane stability which is pertinent in the context of fat absorption by intestinal brush border membrane. The results of this study should also be seen in the context of spontaneous vesiculation, to which considerable theoretical and experimental interest has been devoted recently.

Materials and Methods

Materials

Egg PC was purchased from Lipid Products (Surrey, U.K.), [U-^{14}C]sucrose (spec. act. 9.4 mCi/mmol) from Du Pont de Nemours International (Regensdorf, Switzerland) and calcein from Fluka (Buchs, Switzerland). 1-Monooleoyl-*sn*-glycerol (MOG) was synthesized according to ref. 6. Alternatively, 1-monooleoyl-*rac*-glycerol was purchased from Sigma (St. Louis, MO). Similar results were obtained with synthesized and commercial compounds. 1,2-Dipalmitoyl-*sn*-phosphatidyl[*N-methyl*-^{3}H(U)]choline (^{3}H-DPPC) was synthesized as described [7]. 1-*O*-[9',10'-$^3H_2$]hexadecyl-*sn*-glycerol (^{3}H-hexadecylglycerol) was prepared from 1-*O*-hexadec-9'-enyl-*sn*-glycerol by catalytic tritiation (Amersham International, U.K.). Hexadecenylglycerol was prepared by reacting 2,3-isopropylidene-*sn*-glycerol with hexadecyl methane sulfonate in boiling xylene in the presence of powdered potassium hydroxide, followed by acid-catalyzed removal of the isopropylidene group [8]. The lipids used in this study were pure by TLC standards.

Methods

Mixed EPC/MOG dispersions were made by dissolving the lipids in $CHCl_3$/CH_3OH (2:1, by vol.) and evaporating the solvent by rotary evaporation. The lipids were labeled by adding either ^{3}H-DPPC or ^{3}H-hexadecylglycerol. The lipid film was dried in vacuo and the dried lipid was dispersed in water (pH 6–7) or 1 mM Tris buffer (pH 7.5) by vortexing for 5 min at room temperature. Unless stated otherwise the lipid composition of mixed EPC/MOG dispersions is expressed as weight percent. If desirable [^{14}C]sucrose or calcein were added to the dispersion medium in order to determine the entrapment efficiency of the lipid particles. The final calcein concentration was 0.005 M so that the calcein fluorescence was self-quenched.

Mixed EPC/MOG dispersions containing a trace amount of ^{3}H-DPPC or ^{3}H-hexadecylglycerol in water were subjected to centrifugation at $12000 \times g$ at room temperature for 10 min. If a lipid pellet formed, the supernatant was carefully separated from the pellet by aspiration, and both supernatant and pellet were analyzed for radioactivity. At MOG contents exceeding 40% no lipid pellet formed, but some lipid separated into a turbid, top phase (supernatant phase). In this case the supernatant phase was carefully separated by aspiration from the bottom phase (infranatant phase), and again supernatant and infranatant phase were analyzed for radioactivity. Dispersions of EPC/MOG (1:1, wt. ratio) in water were heated to 50–60 °C for about 1 min which led to the visual clarification of the lipid dispersion. After cooling to room temperature, the lipid dispersion was centrifuged at $12000 \times g$ for 10 min. This treatment produced a clear separation of the turbid, top phase from the clear bottom phase. The top phase was carefully removed from the bottom phase by aspiration and the two phases were analyzed for radioactivity.

Gel filtration on a calibrated Sepharose CL-4B column (50 × 0.9 cm) was carried out as described before [9]. The column was equilibrated and run with 5 mM Tris buffer (pH 7.5) containing 50 mM NaCl and 0.01% NaN_3 (flow rate 7.2 ml/h). The eluate was fractionated with an automatic fraction collector, and each fraction of 0.3 ml was analyzed for radioactive lipids by counting the radioactivity in a Beckman LS-7500 liquid scintillation counter. The calcein content in each fraction was determined by fluorescence spectroscopy. For this purpose each of the 0.3 ml fractions of the eluate was diluted 100 times with 5 mM Tris buffer (pH 7.5) containing 0.02% NaN_3 and cholate was added to a final concentration of 0.2% in order to solubilize the lipid bilayers. The fluorescence intensity of calcein was measured at 520 nm (excitation at 490 nm) with a 5 nm bandpass.

Freeze-fractured samples of lipid dispersions in water were prepared as described before [10]. Proton-decoupled ^{31}P-NMR spectra were recorded on a Bruker CXP-300 Fourier transform spectrometer at 121.46 MHz [11,12]. Axially symmetric ^{31}P powder spectra were recorded using 90° pulses and ^{1}H double resonance conditions with a decoupling power of approx. 100 W. Chemcial shielding was referenced to external 85% orthophosphoric acid. The ^{31}P powder NMR spectra were simulated using Gaussian line shapes according to Seelig [13] and as described in detail before [14]. The error in determining the spectral width of axially symmetric powder patterns was 1 to 2 ppm.

Dynamic light scattering (QLS) was carried out with a Malvern-4700 PS/MW spectrometer and an argon ion laser (Coherent, Innova 200-10, $\lambda_0 = 488$ nm). Measurements were made at a temperature of 25.0 ± 0.1 °C and a scattering angle of 90°. Approximately 1 ml of the lipid dispersion (approx. 1 mg/ml) was transferred into the cylindrical scattering cell (10 mm inner diameter), which was then sealed and subjected to centrifugation at approx. $5000 \times g$ and 25 °C for 20 min. By this procedure dust particles were removed from the scattering volume.

For dilute and monodisperse solutions of small macromolecules, the intensity autocorrelation function $G_2(\tau)$ measured in the dynamic light scattering experi-

ment decays as a single exponential. However, $G_2(\tau)$ cannot be described by a single exponential for polydisperse solutions. Under these conditions, we obtain

$$g_1(\tau) = \int_0^\infty F(\Gamma)\, e^{-\Gamma\tau}\, d\Gamma \quad (1)$$

where $g_1(\tau)$ is the normalized field autocorrelation function (with $g_1(\tau) = [(G_2(\tau) - B)/B]^{1/2}$, B is the experimentally determined base line of the intensity autocorrelation function), $\Gamma = D \cdot Q^2$, D is the translational diffusion coefficient, and Q is the scattering vector ($|Q| = (4\pi n/\lambda_0) \cdot \sin(\theta/2)$, θ being the scattering angle, n the refractive index of the solution, and λ_0 the wavelength of the incident light in vacuo). $F(\Gamma)$ describes the relative light intensity scattered by the particles with diffusion coefficient D, i.e., is a measure of the particle size distribution. A second order cumulant expansion of $G_2(\tau)$ was routinely used to analyze QLS experiments

$$\ln |g_1(\tau)| = -\langle\Gamma\rangle \cdot \tau + \tfrac{1}{2} \cdot \mu_2 \cdot (\Gamma\tau)^2 \quad (2)$$

where $\langle\Gamma\rangle$ is the first cumulant, and μ_2 is a dimensionless quantity which depends on polydispersity [15]. The first cumulant can then be expressed by

$$\langle\Gamma\rangle/Q^2 = \langle D\rangle_z \quad (3)$$

where $\langle D\rangle_z$ is the z-average translational diffusion coefficient. From $\langle D\rangle_z$ an apparent hydrodynamic diameter d_h was calculated using $d_h = k_B T/(3\pi\eta_0\langle D\rangle_z)$, where η_0 is the viscosity of the solvent. A number of correlation functions were further analyzed using a Laplace inversion method by means of an eigenfunction technique [16]. We used a modification of the original method by Ostrowsky et al. [17] which has a substantially improved numerical stability (Schurtenberger, P., unpublished observation). The capability of this data analysis procedure to correctly deconvolute multimodal size distribution has been previously tested with well defined polymer model solutions.

Results

^{31}P-NMR

The effect of increasing concentrations of MOG on the ^{31}P-NMR spectra of unsonicated mixed lipid dispersion of EPC/MOG is shown in Figs. 1 and 2. The top spectrum in Fig. 1 was obtained from an unsonicated aqueous dispersion of EPC. Its line shape is characteristic of a liquid crystalline bilayer with the phosphodiester group undergoing rapid axial averaging about the bilayer normal. The chemical shielding anisotropy $|\Delta\sigma|$ of the resulting axially symmetric ^{31}P powder spectrum is 49 ± 2 ppm in close agreement with published values [13,14,18–20]. The $|\Delta\sigma|$ value

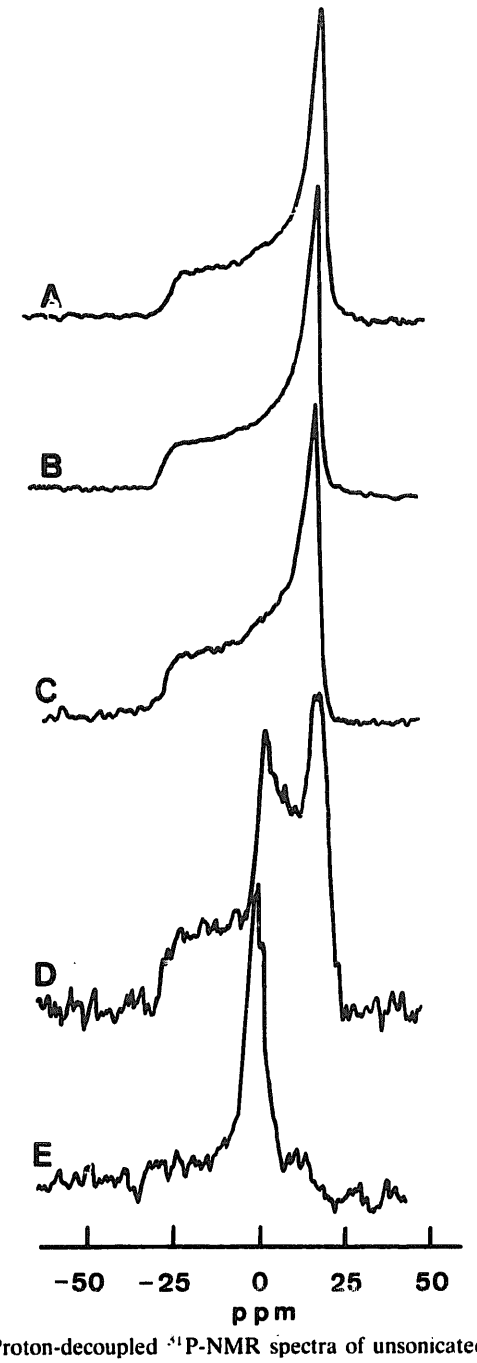

Fig. 1. Proton-decoupled ^{31}P-NMR spectra of unsonicated aqueous dispersions of EPC (A) and EPC containing 10% MOG (B), 40% MOG (C), 50% MOG (D) and 50% MOG at 50 °C (E). Lipids were dispersed in water containing 0.1 mM EDTA as described in Materials and Methods to a final concentration of about 0.2 g/ml ($\approx$ 20%). ^{31}P-NMR spectra were recorded at 25 °C on a Bruker CXP-300 Fourier-transform spectrometer operating at a ^{31}P frequency of 121.46 MHz. 300 to 400 free induction decays were averaged to obtain the spectra shown. A proton-decoupling power of up to 100 W was used. Chemical shielding is expressed in ppm relative to 85% H_3PO_4.

also agrees well with those measured for liquid crystalline unsonicated dispersion in water of 1-palmitoyl-2-oleoyl-*sn*-phosphatidylcholine ($|\Delta\sigma| = 52$ ppm) [21] and 1,2-dipalmitoyl-*sn*-phosphatidylcholine ($|\Delta\sigma| = 49$ ppm) [13,14,20] at 20 °C and 50 °C, respectively. Incor-

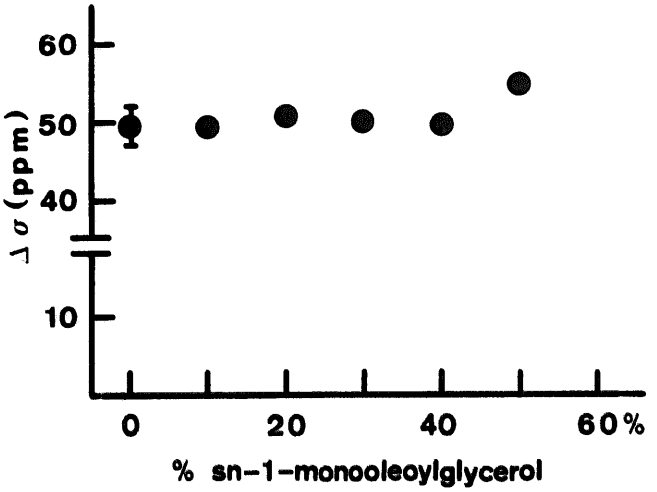

Fig. 2. Chemical shielding anisotropy $|\Delta\sigma|$ as a function of the MOG content. Lipid dispersions were prepared as described in the legends to Fig. 1. Values of $|\Delta\sigma| = \sigma_{\parallel} - \sigma_{\perp}$ were derived either directly from the edges of the ^{31}P powder spectra shown in Figs. 1A–D or by computer simulation of the spectra (data not shown). The $|\Delta\sigma|$ values thus obtained agreed within 1.5 ppm.

poration of increasing quantities of MOG up to about 40 weight% had little effect on lineshape and chemical shielding anisotropy (Figs. 1 and 2). Up to 40 weight% MOG the chemical shielding anisotropy $|\Delta\sigma|$ agreed within experimental error with that of pure EPC (Fig. 2). Mixed EPC/MOG dispersions containing 50 weight% MOG gave composite ^{31}P-NMR spectra (Fig. 1D) consisting of an axially symmetric component of $|\Delta\sigma| \approx 53$ ppm and another component. The second component could be either an isotropic peak at about 2 ppm or alternatively an axially symmetric powder pattern with a peak at the low-field side and a shoulder at the high-field side as is characteristic of hexagonal lipid phases. Due to the cylindrical symmetry of hexagonal phases the chemical shielding anisotropy $|\Delta\sigma|$ will be reduced by a factor of 2 compared to smectic lamellar phases provided the molecular and segmental motions of the lipid molecule are the same in both phases [13]. Based on a lineshape analysis of the ^{31}P-NMR spectrum of Fig. 1D alone it is not possible to differentiate between these two possibilities.

Upon heating the mixed EPC dispersion containing 50 weight% MOG to 50–60 °C the turbidity of the dispersion decreased visually. This process was irreversible: upon cooling the sample to room temperature, the dispersion remained transparent. The ^{31}P-NMR spectrum of an EPC/MOG dispersion (1 : 1, wt. ratio) heated to 50 °C for 1 min and cooled to room temperature is shown in Fig. 1E. The original powder spectrum (Fig. 1D) observed prior to heating collapsed to a single, asymmetric peak at about 1 ppm with a shoulder at the high-field side and a linewidth at half-height of about 700 Hz. This peak may be superimposed on a residual powder pattern (Fig. 1E).

The collapse of the ^{31}P powder NMR spectrum described above is probably due to additional motional averaging of the polar group of EPC induced by heating the mixed EPC/MOG dispersion to 50 °C. Such additional motional averaging could be due to an increase in molecular and/or segmental motion of the phosphodiester group of EPC in the presence of 50% MOG, or to an abrupt change in the average lipid particle size or to a combination of the two mechanisms. Spontaneous vesiculation with the formation of small unilamellar vesicles of a diameter smaller than about 50 nm could account for the observed collapse of the ^{31}P powder spectrum to a single, relatively sharp ^{31}P-NMR signal. For the unambiguous interpretation of the ^{31}P-NMR results, independent evidence from other physical methods is therefore required.

Low-speed centrifugation and gel filtration of mixed EPC / MOG dispersions

Mixed dispersions of EPC/MOG in water or Tris buffer (pH 7.5) at 10 mg/ml labeled with a trace amount of ^{3}H-hexadecylglycerol were centrifuged at $12000 \times g$ at room temperature for 10 min. Under these conditions multilamellar EPC particles sedimented quantitatively. As shown in Fig. 3, practically all the radioactivity was recovered in the lipid pellet. Above a MOG content of 10% the volume of the lipid pellet decreased visually and concomitantly the percentage of radioactivity recovered in the supernatant increased steeply (Fig. 3). At 40% MOG the recovery of radioactivity in the supernatant was almost quantitative (Fig. 3) indicating that the size of lipid particles was reduced to the extent that they no longer sedimented under the centrifugation conditions used. At 50% MOG a great deal of the total lipid ($\approx 50\%$) floated on top of the transparent aqueous lipid dispersion containing $\approx 40\%$ lipid (Fig. 3). The milky top phase and the transparent aqueous lipid phase will be referred to as supernatant and infranatant phase, respectively. A similar separation into a milky top phase (supernatant) and a transparent aqueous phase (infranatant) was induced by briefly heating EPC/MOG dispersion (1 : 1, wt. ratio) to 50–60 °C for 1 min. In order to determine the lipid distribution between supernatant and infranatant phase, EPC/MOG dispersion (1 : 1, wt. ratio) containing either a trace amount of ^{3}H-DPPC or ^{3}H-hexadecylglycerol were heated to about 60 °C for 1 min. The dispersion was then cooled to room temperature and subjected to centrifugation at $12000 \times g$ for 10 min. The milky supernatant was carefully removed by aspiration and the radioactivity of both supernatant and infranatant phases was determined. The results of three measurements are summarized in Table I. The wt. ratio of EPC/MOG in the supernatant and infranatant phase was calculated as 0.61 and 1.75, respectively, based on the assumption

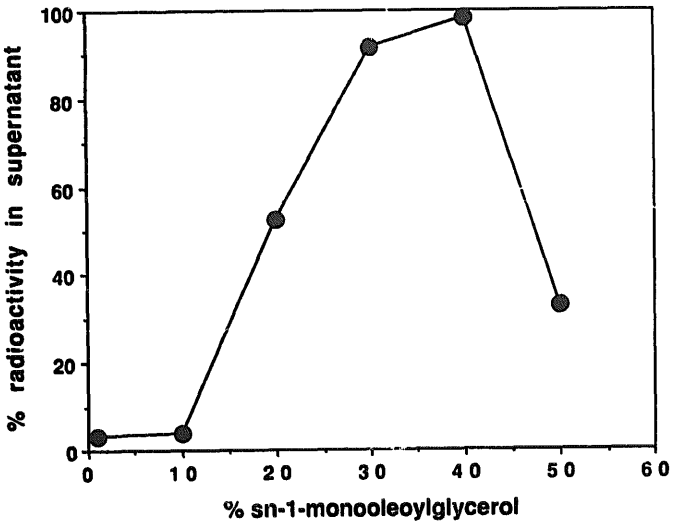

Fig. 3. Mixed EPC/MOG dispersions in water at 10 mg total lipid/ml were prepared as described in Materials and Methods. Each lipid dispersion was labeled with a trace amount of ^{3}H-hexadecylglycerol. The mixed EPC/MOG lipid dispersions were centrifuged at 12000×*g* at room temperature for 10 min. The supernatant was separated from the lipid pellet by aspiration and analyzed for radioactive lipid. The radioactivity recovered in the supernatant expressed as percent is plotted as a function of the MOG content (%) of the mixed lipid dispersion.

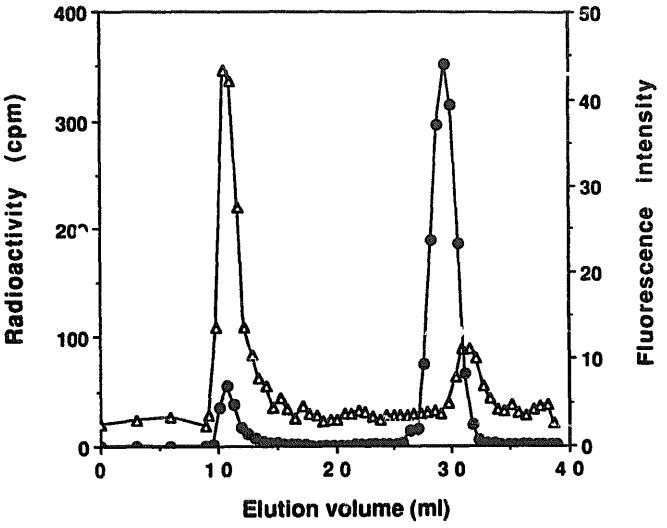

Fig. 4. Gel filtration of a mixed EPC/MOG dispersion (1:1, wt. ratio) obtained on Sepharose CL-4B. A mixed lipid dispersion of EPC/MOG (1:1, wt. ratio) and a trace amount of ^{3}H-DPPC was made as described in Materials and Methods. The dispersion (total lipid concentration 10 mg/ml) was heated to 55°C for 1 min and centrifuged at 12000×*g* for 10 min. 0.3 ml of the clear infranatant lipid dispersion was applied to the Sepharose CL-4B column (50×0.9 cm) which was equilibrated and run with 5 mM Tris buffer (pH 7.5) containing 50 mM NaCl and 0.01% NaN_3 at a flow rate of 7.2 ml/h. The eluate was fractionated in a fraction collector and each fraction of 0.3 ml was analyzed for radioactivity and calcein fluorescence as described in Materials and Methods. Lipid concentration determined as radioactivity (cpm) (△) and fluorescence intensity of calcein (●).

that the distribution of the two radiolabels approximates the distribution of the bulk lipids. The enrichment of MOG in the supernatant phase is even more obvious if the results are expressed as mole ratios of MOG/EPC (Table I, numbers in parenthesis).

The transparent aqueous lipid phase (infranatant) prepared as described above was analyzed by gel filtration on Sepharose CL-4B. A typical elution pattern of the infranatant phase of a mixed EPC/MOG dispersion (1:1, wt. ratio) is shown in Fig. 4. The lipid particles eluted as an asymmetric peak in the column void volume indicating that the diameter of the particles exceeds 60 nm. There is a second minor lipid peak at about the total column volume. The nature of this peak was not further investigated. From its position it is assumed that it arises from lipid degradation induced by heating the lipid to 50–60°C. Information concerning the nature of the lipid particles of the main peak (Fig. 4) was obtained by adding [^{14}C]sucrose or calcein to the dispersion medium. If [^{14}C]sucrose or calcein was present in the dispersion medium, about 2–5% of the total sucrose or calcein were coeluted with the lipid peak (Fig. 4). The coelution of these small molecules with the main lipid peak suggests that the lipid particles are vesicles with a water-filled, internal cavity. The entrapment values of several percent are consistent with large unilamellar vesicles.

Fractions of the main lipid peak (Fig. 4) were pooled and concentrated to about 1 mg lipid/ml using Amicon filtration equipment and YM10 Amicon filters. The dispersion thus obtained was stored at 4°C for about 30 days. No fluorescence developed under these conditions indicating that the EPC/MOG vesicles were stable. Any instability of the vesicles, e.g., vesicle fusion can be assumed to be accompanied by leakage of calcein, and such a leakage would have been readily detected by an increase in fluorescence intensity.

TABLE I

Radioactivity recovered in the two phase system of mixed EPC/MOG dispersions (1:1, wt. ratio)

Mixed EPC/MOG (1:1, wt. ratio; 0.48, mole ratio) dispersions in water were prepared as detailed in Materials and Methods and treated as described in the text.

Phase	Radioactivity (%)		wt. ratio (mole ratio) MOG/EPC
	^{3}H-hexadecyl-glycerol	^{3}H-DPPC	
Supernatant	70±6	43±3	1.63 (3.34)
Infranatant	32±3	56±5	0.57 (1.21)

Freeze-fracture electron microscopy

Electron micrographs of freeze-fractured samples of mixed EPC/MOG dispersions in water up to 10% MOG revealed large, multilamellar particles (Fig. 5a). These particles closely resemble those present in multilamellar EPC dispersions. Consistent with this finding

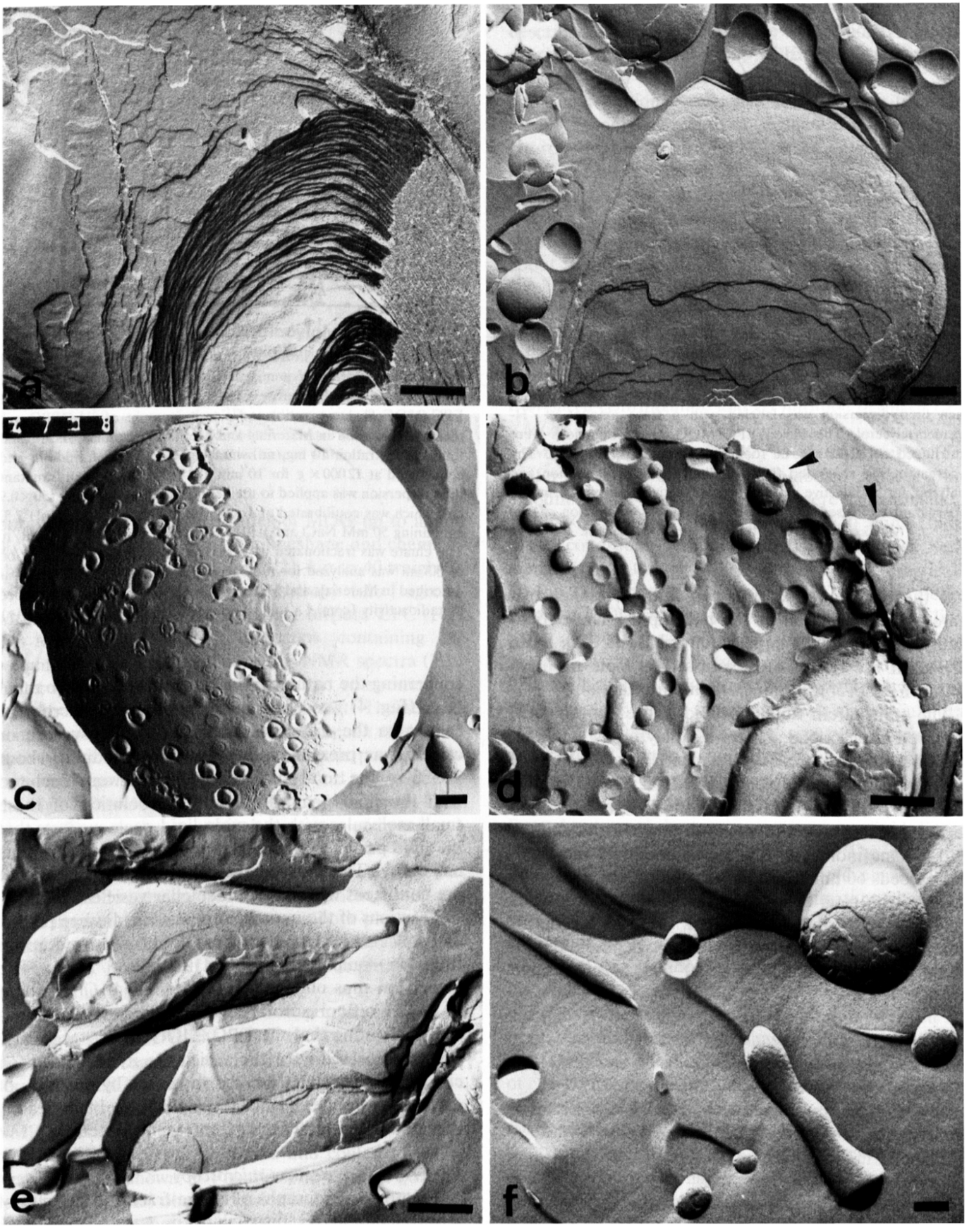

Fig. 5. Electron micrographs of freeze-fractured mixed EPC/MOG dispersions in H_2O at a total lipid concentration of 10 mg/ml. EPC containing 10% MOG (a), 40% MOG (b), 50% MOG (c and d). Supernatant (e) and infranatant phase (f) of a mixed EPC/MOG dispersion in H_2O (1 : 1, wt. ratio) were obtained as described in the text.

is the observation that the particles of mixed EPC/MOG dispersions containing up to about 10% MOG sedimented readily when centrifuged at 12000 × *g* for 10 min (cf. Fig. 3). In mixed EPC/MOG dispersions containing more than 10% MOG, the particle size distribution changed with increasing MOG content: the multilamellar particles of diameter larger than 1 μm were gradually replaced by smaller oligolamellar and unilamellar vesicles of a size mostly in the range of 100 nm to 1 μm (Figs. 5b–d). The shape of these vesicles is often spherical, but elongated and irregularly shaped bodies are also seen (Figs. 5b–d). The polydispersity of these dispersions was such that a meaningful application of QLS was not possible. The particles present in EPC/MOG dispersions containing more than 10% MOG, particularly the large ones, exhibit fracture faces quite different from the smooth fracture faces of pure EPC dispersions. First, the fracture faces are covered with numerous more or less spherical, shallow cavities and protrusions which probably result from the budding process of smaller vesicles (Fig. 5c). Such budding process can be seen in cross-section in Fig. 5d (see arrows). Secondly, the plane of fracture appears to alternate frequently between different lipid lamellae giving rise to a rough fracture face (cf. Figs. 5a and b).

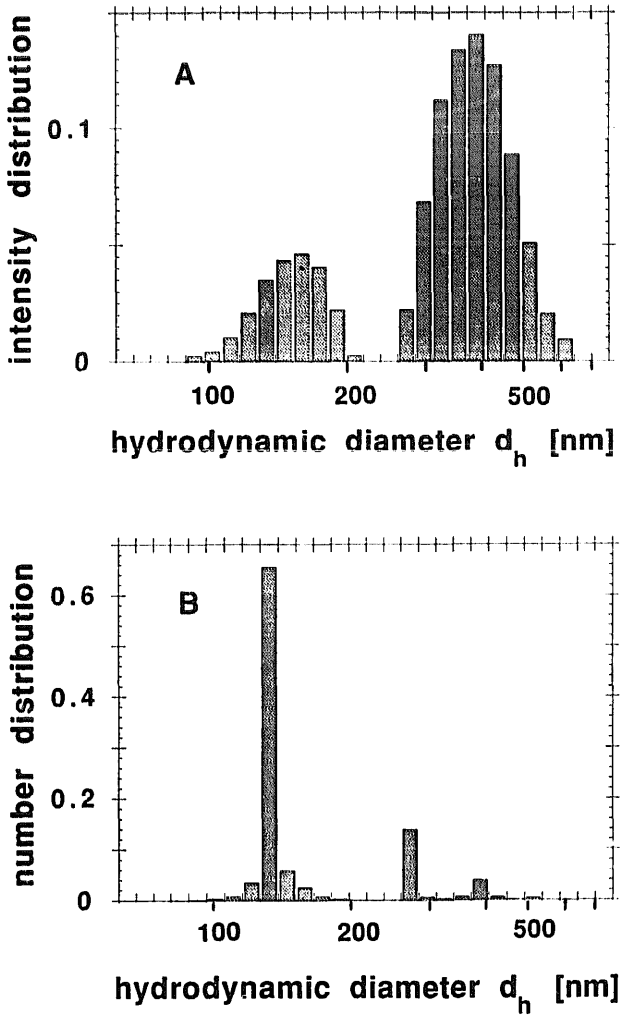

Fig. 6. Dynamic light scattering (QLS) of a mixed EPC/MOG dispersion (1:1, wt. ratio). The fraction of light scattered is shown as a function of the vesicle hydrodynamic diameter (on a logarithmic scale) (A) together with an estimate of the number distribution function $f(d_h)$ (B). EPC/MOG (1:1, wt. ratio) was dispersed in water or 1 mM Tris buffer pH 7.5 as described in Materials and Methods. The dispersion was heated to about 60 °C for 1 min, which caused clearing of the milky dispersion to a transparent one. The dispersion was centrifuged at 12000× *g* for 10 min, and the clear infranatant (about 10 mg/ml) was 10-times diluted and analyzed by QLS.

Mixed, aqueous EPC/MOG dispersions (1:1, wt. ratio) were briefly heated to 50 °C and centrifuged at 12000 × *g* for 10 min as described in Materials and Methods. Supernatant and infranatant phases thus produced were separated and both phases were examined by freeze-fracture electron microscopy. The supernatant consisted of large multilamellar and oligolamellar particles of a diameter of 100 nm to several μm (Fig. 5e). The infranatant phase contained largely unilamellar vesicles in the size range of 100 to 300 nm. Some elongated and oligolamellar particles were also present (Fig. 5f). The infranatant lipid dispersion was chromatographed on Sepharose CL-4B as described in Fig. 4. The lipid eluted in the void volume was collected, pooled and concentrated to 1 mg lipid/ml as described above. Electron microgrpahs of freeze-fractured samples of such lipid dispersions revealed mainly large unilamellar vesicles with a size distribution ranging between 100 and 500 nm (data not shown). Mixed EPC/MOG dispersions containing 60% MOG consisted mainly of unilamellar and oligolamellar vesicles of sizes between 100 and 1000 nm (data not shown).

Dynamic light scattering (QLS)

Results of gel filtration and freeze-fracture electron microscopy indicate that mixed dispersions of EPC/MOG (1:1, wt. ratio) are polydisperse consisting of large unilamellar and oligolamellar particles. The particle size distribution of such dispersions was further analyzed by QLS. A cumulant analysis yielded an average value of $d_h \approx 280$ nm, and indicated a relatively high degree of polydispersity. A careful analysis of the intensity autocorrelation functions with the Laplace inversion program reproducibly resulted in a bimodel size distribution with peaks at $d_h = 120 \pm 40$ nm and $d_h = 360 \pm 120$ nm, respectively. A characteristic example of the results from such an analysis of the vesicle size distribution is shown in Fig. 6. This figure shows the fraction $F(d_h)$ of light scattered as a function of the hydrodynamic diameter d_h, i.e., an intensity-weighted size distribution of the vesicles. At least a qualitative estimate of the number of vesicles present in the two populations can be obtained from their relative contributions to the total scattering intensity.

For polydisperse vesicles, the average intensity in the absence of interparticle interaction effects can be computed according to

$$I(Q) \approx V_p \int_0^\infty V(d,t)^2 P(Q,d,t) f(d)\, dd \quad (4)$$

where V_p is the number density of vesicles, $V(d,t)$ is the volume and $P(Q,d,t)$ is the scattering form factor of a spherical shell of diameter d and shell (bilayer) thickness t, and $f(d)$ is the normalized particle number distribution function describing the size distribution of the particles [22]. Using $d = d_h$ we thus obtain the following expression for the intensity distribution $F(d_h)$

$$F(d_h) = V(d_h,t)^2 P(Q, d_h, t) f(d_h) \Big/ \int_0^\infty V(d_h,t)^2 P(Q,d_h,t) f(d_h)\, dd_h \quad (5)$$

which in turn permits an estimate of the number ratio $f(d_{h,1})/f(d_{h,2})$ of the vesicles in peak 1 and 2 from $F(d_{h,1})/F(d_{h,2})$ though

$$\frac{f(d_{h,1})}{f(d_{h,2})} = \frac{F(d_{h,1})}{F(d_{h,2})} \cdot \frac{V(d_{h,2},t)^2 P(Q, d_{h,2}, t)}{V(d_{h,1},t)^2 P(Q, d_{h,1}, t)} \quad (6)$$

If we now use the experimentally determined values of d_h and $F(d_h)$ for the two populations of vesicles, we can estimate that the number of smaller vesicles with $d_h = 120$ nm is approx. 10-times higher than that with $d_h = 360$ nm. The size distribution $f(d_h)$ thus determined is shown in Fig. 6b. This result is at least qualitatively consistent with the results of freeze-fracture electron microscopy, where we see predominantly vesicles with a diameter of approx. 100–150 nm, and a significantly smaller number of larger vesicles.

Discussion

The main conclusions which can be drawn from the experiments presented are as follows:

EPC bilayers have a remarkable capacity of accommodating large amounts of MOG. Up to 40% MOG (1.4, mole ratio MOG/EPC) are incorporated without significantly affecting the orientation and motion of the polar group of EPC (cf. Fig. 1). Up to the highest MOG content used here (≈ 70% MOG) corresponding to a MOG/EPC mole ratio of 3.4 (cf. Table I) the lamellar (bilayer) phase is maintained. Even in excess MOG the bilayer is the most stable structure (cf. Fig. 5). The phase behaviour of mixed EPC/MOG dispersions described here is consistent with the phase diagram reported before [39].

Upon heating mixed EPC/MOG dispersions of wt. ratio 1 (2.1, mole ratio MOG/EPC) to 50–60 °C, the turbidity of the dispersion decreased abruptly. Evidence from different physical methods taken together indicates that at this point large multilamellar particles are dispersed to smaller oligolamellar and unilamellar vesicles. This process of dispersion may be viewed as spontaneous vesiculation for it matches the criteria used to define spontaneous vesiculation [23–28]. Multilamellar stacks represent the most stable structure of aqueous dispersions of pure phosphatidylcholines. Diluting isoelectric EPC molecules with neutral MOG molecules to a final EPC/MOG wt. ratio ≤ 1 apparently induces budding of vesicles as shown in the electron micrographs of Figs. 5c and d. The resulting large unilamellar vesicles of diameter greater than 100 nm are probably the most stable (equilibrium) structure under these conditions. Residual oligolamellar structures observed (cf. Figs. 5c–f) may represent metastable states. Freeze-fracture electron microscopy and QLS show that the resulting vesicles are polydisperse with diameters ranging from 100 to 1000 nm. The bulk of the vesicles are between 100 to 500 nm (Figs. 5 and 6). This result is consistent with gel filtration on Sepharose CL-4B showing that the average diameter of the vesicles exceeds 60 nm. The gel filtration experiment rules out the presence of a significant proportion of small unilamellar vesicles of diameter smaller than 50 nm.

The visual clearance of EPC/MOG dispersions (1 : 1, wt. ratio) upon heating is accompanied by a collapse of the ^{31}P powder NMR spectrum to a fairly narrow, slightly asymmetric resonance (Fig. 1E). The evidence presented indicates that heating of mixed EPC/MOG dispersions (1 : 1, wt. ratio) induces spontaneous vesiculation with the formation of unilamellar and oligolamellar vesicles of a size range of 100 to 1000 nm. However, the reduction in particle size from several micrometers to vesicles of submicrometer size cannot be the explanation for the collapse of the ^{31}P powder pattern. Aqueous dispersion of ox brain phosphatidylserine (10 mg/ml) have been shown to consist to more than 90% of unilamellar vesicles with diameters smaller than 1000 nm [29]. Such dispersions give typical ^{31}P powder NMR spectra at room temperature characteristic of liquid crystalline bilayers [12] with no indication of a sharp isotropic signal superimposed on the powder pattern. By analogy with this result, the vesicles present in mixed EPC/MOG dispersions (1 : 1, wt. ratio) after heating are expected to give rise to a ^{31}P powder pattern. Since this is not the case, additional molecular and segmental motions of the EPC polar group have to be implicated in order to account for the observed collapse of the ^{31}P powder NMR spectrum. Alternatively, a change in the motionally averaged orientation of the phospholipid polar group with respect to the bilayer normal or director axis could also account for the collapse of the ^{31}P powder NMR spectrum. We favour the former explanation

that at high MOG contents (1 : 1, wt. ratio, corresponding to a mole ratio MOG/EPC ≈ 2) additional motional averaging of the EPC polar group is responsible for the observed narrowing of the ^{31}P-NMR signal. It was shown that the orientation of the polar group of phosphatidylcholine is determined primarily by intramolecular forces [30] and that this preferred 'conformation' is energetically fairly stable. It would require strong intermolecular interactions between EPC and MOG to induce conformational and orientational changes in the phospholipid polar group. None of the experiments carried out here testify to a particularly strong interaction between the polar groups of EPC and MOG. Furthermore, if indeed the presence of MOG induces an increase in the motional freedom of the EPC polar group, this effect should be detectable by ESR spin labeling. For this purpose spin-labeled phosphatidylcholine (1-palmitoyl-2-[5-doxylstearoyl]-3-*sn*-phosphatidylcholine) was incorporated in EPC bilayers and mixed EPC/MOG bilayers (1 : 1, wt. ratio, 100 : 1, EPC/spin label, mole ratio). In both cases anisotropic ESR spectra were obtained which are characteristic for rapid but anisotropic motion (data not shown). From these spectra order parameters S were derived using standard methods [31]. For EPC bilayers corrected order parameter at room temperature thus obtained was $S = 0.64 \pm 0.01$ in good agreement with data in literature [32]. In the mixed EPC/MOG bilayer the order parameter decreased to $S = 0.57 \pm 0.01$ confirming that the presence of MOG in EPC bilayers loosens the molecular packing in the lipid polar group. This effect is apparently propagated to the neighbouring hydrocarbon chain region and sensed by the spin label probing this region. We propose therefore that the visual clearance of mixed EPC/MOG dispersions induced by briefly heating mixed EPC/MOG (1 : 1, wt. ratio) dispersions to 50–60 °C reflects the dissolution of multilamellar lipid stacks which are being replaced mainly by large unilamellar vesicles. The collapse of the ^{31}P-NMR powder pattern is likely to be due to an increase in the motional freedom of the phospholipid polar group in the presence of MOG. The spontaneous budding of vesicles and also the irregularly shaped particles observed with mixed EPC/MOG dispersions (wt. ratio ≤ 1) suggests that the mechanical properties of these mixed bilayers are significantly different from those of pure EPC bilayers. The vesicles found in mixed EPC/MOG (1 : 1, wt. ratio) have the ability to entrap small molecules such as sucrose and calcein. Their entrapment capacity is consistent with the average size of these vesicles determined by electron microscopy and QLS. The encapsulation experiment using calcein provides evidence for the stability of these vesicles. The EPC/MOG bilayer remains impermeable for calcein when these vesicles are stored at 4 °C for 1 month.

At high MOG contents (≥ 50%), low-speed centrifugation produced creaming of the dispersion with the separation of a milky top phase. Freeze-fracture electron microscopy shows that this phase is still smectic lamellar consisting of multilamellar and oligolamellar lipid particles. The data summarized in Table I indicate that these particles are enriched in MOG. Apparently, the way the mixed EPC/MOG dispersions were prepared does not ensure the perfect mixing of the two lipids. Furthermore, there appears to be also incomplete mixing within the plane of the bilayer as evident from freeze-fracture electron microscopy (Figs. 5c and d). At MOG contents ≥ 40% shallow protrusions and cavities can be seen on the lipid fracture faces. These structures that have never been observed with pure EPC bilayers may reflect inhomogeneities in the lateral distribution of EPC and MOG.

Physiological significance

Monoacylglycerols are represented by two chemical species: (1) the *sn*-1 or *α*-monoacylglycerols and (2) the *sn*-2 or *β*-monoacylglycerols. Acyl migration is known to lead to an equilibrium in which 80–90% are present as the *sn*-1-compound [33]. From the work published on the physical-chemical properties of monoacylglycerols (for a review see Ref. 33), it is not clear whether there are significant differences between *sn*-1 and *sn*-2-monoacylglycerols. Larsson [34] reported that 2-decanoyl- and 2-hexadecanoyl-*sn*-glycerol exhibit the same phase behaviour as the corresponding *sn*-1 compounds except for the lower melting points of the *sn*-2-compounds. This finding suggests that the two types of monoacylglycerols may behave similarly, at least regarding their phase behaviour. A common feature of the physical-chemical properties of *sn*-1 and *sn*-2-monoacylglycerols is the preference for smectic (lamellar) phases. This is true for the anhydrous as well as the hydrated state [33–38]. 2-Acyl-*sn*-glycerols and fatty acids are the main products of fat (triacylglycerol) digestion [4]. It is probably of physiological significance that both lipolytic products have a preference for the smectic (lamellar) phase [33]. As mentioned in the introduction, during fat digestion and absorption, high concentrations of both lipolytic products may be present in the intestinal lumen and in turn in brush border membrane, particularly following a fatty meal. In this context the question arises how the incorporation of large quantities of monoacylglycerols and fatty acids, though transient, affect the structure and function of brush border membrane. The work presented here is pertinent to this question. We have shown that large quantities of monoacylglycerols can be accommodated in lipid bilayers without significantly perturbing the lipid packing and without inducing a phase change to a non-lamellar phase. Extrapolating this finding to brush border membrane, we propose that brush border mem-

brane may incorporate monoacylglycerols (and probably also fatty acids) at fairly high concentrations during lipid absorption with a minimum perturbation in the lipid packing. Whatever the local perturbation of the lipid environment may be, it must be such that the barrier and other functional properties of the brush border membrane are still maintained.

Acknowledgement

This work was supported by the Swiss National Science Foundation (Grant No. 31-25719.88).

References

1 Hernell, O., Staggers, J.E. and Carey, M.C. (1990) Biochemistry 29, 2041–2056.
2 Borgström, B. (1977) Int. Rev. Physiol. 12, 305–323.
3 Patton, J.S. (1981) in Physiology of the Gastrointestinal Tract (Johnson, L.R., ed.), pp. 1123–1146, Raven Press, New York.
4 Carey, M.C., Small, D.M. and Bliss, C.M. (1983) Annu. Rev. Physiol. 45, 651–677.
5 Thomson, A.B.R. and Dietschy, J.M. (1981) in Physiology of the Gastrointestinal Tract (Johnson, L.R., ed.), pp. 1147–1220, Raven Press, New York.
6 Buchnea, D. (1971) Lipids 6, 734–739.
7 Thurnhofer, H. and Hauser, H. (1990) Biochim. Biophys. Acta 1024, 249–262.
8 Baumann, W.J. and Mangold, H.K. (1964) J. Org. Chem. 29, 3055–3057.
9 Schurtenberger, P. and Hauser, H. (1984) Biochim. Biophys. Acta 778, 470–480.
10 Hauser, H., Gains, N. and Müller, M. (1983) Biochemistry 22, 4775–4781.
11 Casal, H.L., Mantsch, H.H., Demel, R.A., Paltauf, F., Lipka, G. and Hauser, H. (1990) J. Am. Chem. Soc. 112, 3887–3895.
12 Hauser, H., Mantsch, H.H. and Casal, H.L. (1990) Biochemistry 29, 2321–2329.
13 Seelig, J. (1978) Biochim. Biophys. Acta 515, 105–140.
14 Gally, H.-U., Niederberger, W. and Seelig, J. (1975) Biochemistry 14, 3647–3652.
15 Koppel, D.E. (1972) J. Chem. Phys. 57, 4814–4820.
16 McWhirter, J.G. and Pike, E.R. (1978) J. Phys. (A) 11, 1729–1745.
17 Ostrowsky, N., Sornette, D., Parker, P. and Pike, E.R. (1981) Optica Acta 28, 1059–1071.
18 Cullis, P.R., De Kruijff, B. and Richards, R.E. (1976) Biochim. Biophys. Acta 426, 433–446.
19 Kohler, S. and Klein, M.P. (1977) Biochemistry 16, 519–526.
20 Hauser, H. (1981) Biochim. Biophys. Acta 646, 203–210.
21 Tamm, L. and Seelig, J. (1983) Biochemistry 22, 1474–1483.
22 Schurtenberger, S. and Hauser, H. (1992) in Liposome Technology, 2nd Edn. (Gregoriadis, G., ed.), in press, CRC Press, Boca Raton.
23 Rydhag, L. and Gabran, T. (1982) Chem. Phys. Lipids 30, 309–324.
24 Rydhag, L., Stenius, P. and Oedberg, L. (1982) J. Colloid. Interface Sci. 86, 274–276.
25 Hauser, H. and Gains, N. (1982) Proc. Natl. Acad. Sci. USA 79, 1683–1687.
26 Mantelli, S., Speiser, P. and Hauser, H. (1985) Chem. Phys. Lipids 37, 329–343.
27 Hauser, H., Gains, N., Eibl, H.-J., Müller, M. and Wehrli, E. (1986) Biochemistry 25, 2126–2134.
28 Hauser, H. (1987) Chem. Phys. Lipids 43, 283–299.
29 Atkinson, D., Hauser, H., Shipley, G.G. and Stubbs, J.M. (1974) Biochim. Biophys. Acta 339, 10–29.
30 Hauser, H., Guyer, W., Pascher, I., Skrabal, P. and Sundell, S. (1980) Biochemistry 19, 366–373.
31 Seelig, J. (1976) in Spin Labeling Theory and Application (Berliner, L.J., ed.), pp. 373–409, Academic Press, New York.
32 Barrat, M. and Laggner, P. (1974) Biochim. Biophys. Acta 363, 127–133.
33 Small, D. (1986) in The Physical Chemistry of Lipids. From Alkanes to Phospholipids, pp. 386–392, Plenum Press, New York.
34 Larsson, K. (1967) Z. Phys. Chem. 56, 173–198.
35 Larsson, K. (1964a) Ark. Kemi 23, 23–27.
36 Larsson, K. (1964b) Ark. Kemi 23, 29–33.
37 Larsson, K. (1966) Acta Crystallogr. 21, 267–272.
38 Kodali, D.R., Redgrave, T.G., Small, D.M. and Atkinson, D. (1985) Biochemistry 24, 519–25.
39 Gutman, H., Arvidson, G., Fontell, K. and Lindblom, G. (1984) in Surfactants in Solution (Mittal, K.L. and Lindman, B., eds.), Vol. 1, pp. 143–152, Plenum Press, New York and London.